ChemComm

Accepted Manuscript

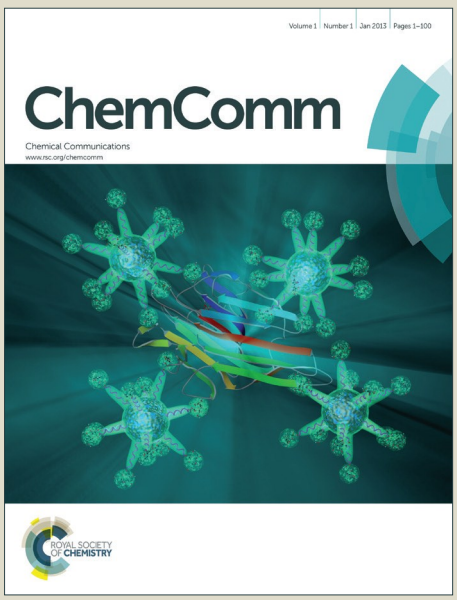

ROYAL SOCIETY OF CHEMISTRY

www.rsc.org/chemcomm

Journal Name

COMMUNICATION

Three-Dimensional Hyperbranched PdCu Nanostructures with High Electrocatalytic Activity

Received 00th January 20xx,
Accepted 00th January 20xx

DOI: 10.1039/x0xx00000x

www.rsc.org/

Bo Jiang,[a,b] Cuiling Li,[*a] Victor Malgras,[a] Yoshio Bando[a] and Yusuke Yamauchi[*a,b]

In this study, three-dimensional (3D) PdCu alloyed nanostructures, consisting of one-dimensional (1D) branches, were successfully synthesized through a facile wet-chemical method without using any seeds or organic solvent. The success of this approach relies on the use of hydrochloric acid (HCl) to control the reduction rate, and on the presence of bromide ions (Br^-) to selectively adsorb on the certain facets of the PdCu nucleus. The as-prepared 3D PdCu nanostructures exhibit greatly enhanced catalytic activity toward formic acid oxidation, owing to a suitable electronic landscape resulting from the alloy structure and the unique morphology.

In the past decades, fuel cells have been considered as promising devices for energy conversion owing to their high efficiency, low operation temperatures, and low pollutant emissions.[1] Presently, platinum (Pt) nanomaterials are still the most efficient electrocatalysts for both anodic and cathodic reactions. The commercialization of fuel cells has been obstructed by the high cost of Pt and the limited reserves in nature. Recent advances demonstrated that porous/dendritic Pt crystals,[2] core-shell nanoparticles with monolayer Pt shell,[3] and Pt-based alloys with other transition metals[4] can effectively decrease the usage of Pt while still maintaining the possibility to enhance the performance. However, these approaches only reduce the usage of Pt, and do not fully solve the problem of Pt requirements.[5] Therefore, the development of less expensive and more abundant Pt-free electrocatalysts with improved catalytic activity and durability is still an urgent matter to address.

Palladium (Pd) and Pd-based catalysts represent promising substitutes to Pt for catalyzing oxidation of small fuel molecules due to their relatively low cost and abundance. Especially, Pd has exhibited superior activity in catalyzing formic acid oxidation (FAO) through a direct oxidation process (a direct dehydrogenation pathway) without poisonous intermediates (carbon monoxide), which is distinctly different from Pt-based catalysts.[6] However, it should be mentioned that the Pd atoms on the surface easily dissolve and migrate during reactions taking place in acid solution, resulting in the aggregation of the nanoparticles and in the loss of surface area and activity.[7] Recent experimental results indicated that three-dimensional (3D) constructions composed of one-dimensional (1D) metallic nanostructures (*e.g.* nanorods, nanowires, and nanodendrites/branches) can be considered as effective candidates to improve the activity and stability of fuel cells.[8] Such kind of assembly not only retains the inherent anisotropic 1D morphology, which suffers less from dissolution and Ostwald ripening/aggregation,[9] but also has many unique structural characteristics such as the porosity, the permeability, and interconnected open-pore structures to enhance the catalytic activity and stability.[10] For instance, Xia *et al.* reported that the interconnected 3D Pt nanowire assemblies exhibited significant enhanced electrocatalytic activity and durability for methanol oxidation reaction compared with a commercial Pt/C catalyst because of their unique architecture.[11] Besides the structure, embedding non-precious-metal atoms into Pd lattice to form the Pd-based alloy catalysts is another effective strategy to enhance the activity and stability owing to the modulation of the electronic configuration.[12] The synthesis of mono-dispersed PdCo and PdCu nanoparticles with a controlled composition was reported by Ho et al. The latter exhibits an enhanced Pd mass activity toward FAO, which is about 2 times higher than that of Pd catalyst, owing to the effect of Cu on the electronic landscape of the PdCu alloy structure.[13]

Despite the significant progress made in the synthesis of bimetallic Pd-based alloy, produce branched Pd-based alloy with 3D structures remains a challenge as the face-centered-cubic (fcc) Pd structure has no intrinsic driving force towards the growth of anisotropic structure in solution phase.[14] 3D branched PdCu nanostructures are less vulnerable to aggregation and dissolution and can decrease the Pd

[a] *World Premier International (WPI) Research Center for Materials Nanoarchitectonics (MANA) National Institute for Materials Science (NIMS) 1-1 Namiki, Tsukuba, Ibaraki 305-0044 (Japan).*
[b] *Faculty of Science and Engineering, Waseda University 3-4-1 Okubo, Shinjuku, Tokyo 169-8555 (Japan).*
Electronic Supplementary Information (ESI) available: [details of any supplementary information available should be included here]. See DOI: 10.1039/x0xx00000x

consumption and increase the utilization of Pd. Thus, it is essential to develop bimetallic Pd-based catalyst with 3D architectures composed of 1D metallic nanostructure to maximize their performance and increase their catalytic stability.

Herein, we demonstrated a facile one-step method for the preparation of three-dimensional alloyed PdCu nanostructures composed of 1D branches. The impact of the reagents on the formation of such 3D PdCu nanostructure is investigated in details. The results indicate that the slow reduction kinetics retarded by the presence of hydrochloric acid (HCl) and the bromide ions (Br^-) adsorbing selectively on certain facets of the PdCu seeds during the reduction progress are key factors for the successful formation of 3D branched PdCu nanostructures. More importantly, because of the unique structural advantage and the incorporation of Cu atoms, the as-prepared 3D branched PdCu nanostructures show enhanced catalytic activity compared with the commercial Pd black (PdB) and PdC-10%.

In a typical synthesis of 3D branched PdCu nanostructures, 1.5 ml Na_2PdCl_4 solution (20.0 mM), 1.5 ml $CuCl_2$ solution (20.0 mM), 0.1 ml HCl solution (6.0 M), 80 mg KBr and 50.0 mg Pluronic F127 were mixed and dissolved under sonication. An aqueous solution of 2.0 ml ascorbic acid (0.1 M) was added to the solution which was then kept in an oil bath for 30 min at 90 ^{o}C. The residual Pluronic F127 was removed by several consecutive washing/centrifugation cycles with ethanol and water. Finally, the sample was collected by centrifuging at 14000 rpm for 20 min. The as-prepared sample was stored in ethanol until the time of use and then dried at room temperature.

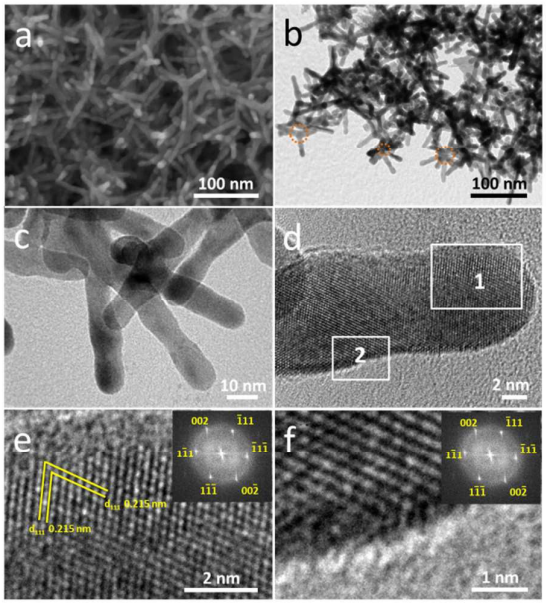

Fig. 1 a) Representative SEM and b, c) TEM images of the 3D branched PdCu nanostructures, d) HRTEM image of a single-crystal PdCu branch, e, f) Magnified HRTEM images of the edge surface derived from the rectangle areas marked in (d), respectively. The corresponding FFT patterns were shown as inset in panel (e, f).

The morphology of the obtained products is examined by scanning electron microscope (SEM) and transmission electron microscopy (TEM). As shown in **Fig. 1a**, the as-prepared products display highly branched 3D multipods. The TEM images reveal that each PdCu nanostructure consists of 3-7 branches **(Fig. 1b,c)**. The width and the length of the branches are in the range of 8-11 nm and 20-50 nm, respectively. The branches originating from a same center extend in different directions to form a 3D structure, as marked in **Fig. 1b**. The detailed structural features of the branches were characterized by high-resolution TEM (HRTEM), as shown in **Fig. 1d**. The lattice spacing of the 3D branched PdCu nanostructures **(Fig. 1e)** was measured to be around 0.215 nm, which is between the {111} lattice spacing of pure Pd (0.223 nm) and Cu (0.208 nm), indicating the successful incorporation of Cu atoms into the Pd lattice. The continuous fringes running through the branches suggest that they are monocrystalline. The Fourier transform (FFT) patterns of the atomic lattice fringes were identical, as displayed in the insets of **Fig. 1e** and **f**, further supporting the monocrystalline nature of the branched PdCu nanostructures.

The elemental mapping images (**Fig. 2a-d**) confirm that the Pd and Cu are uniformly distributed throughout the branch, which suggests the formation of a homogeneous PdCu alloy structure. In addition, the energy dispersive X-ray spectroscopy (EDS) also returns a Pd:Cu atomic ratio of 80:20, although an equal feeding molar ratio was utilized, in accordance to the inductively coupled plasma atomic emission spectrometry data (ICP-AES), indicating that the reduction of the Cu species was incomplete. The possible reason is that the Cu^{2+} species (Cu^{2+}/Cu=0.34 V *vs*. Standard Hydrogen Electrode, SHE) have a lower reduction potential than that of Pd^{2+} ($[PdCl_4]^{2-}$/Pd: +0.62 V *vs*. SHE).[15]

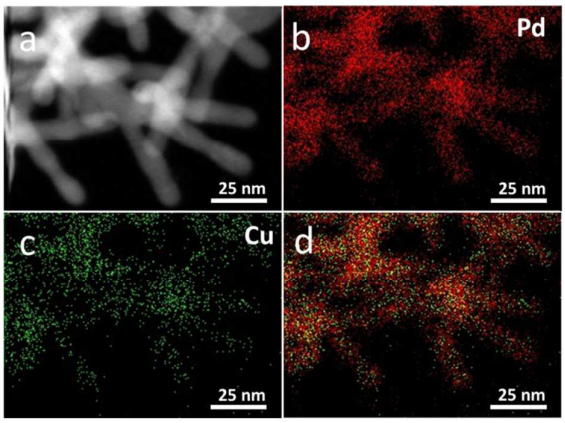

Fig. 2 a) HAADF-STEM and b-d) elemental mapping images of the 3D branched PdCu nanostructures.

The crystalline structure of the typical 3D branched PdCu nanostructures was examined by wide-angle X-ray diffraction (XRD). As shown in **Fig. S1**, the diffraction peaks of the PdCu sample at 40.5 ^{o}, 47.1 ^{o}, 68.9 ^{o}, 83.2 ^{o}, 87.8 ^{o} can be clearly assigned to the (111), (200), (220), (311), and (222) diffraction planes, respectively. No other diffraction peaks were observed,

indicating the formation of a single-phase PdCu alloy. When compared to standard diffraction patterns of Pd, all the diffraction peaks of the 3D branched PdCu nanostructures are shifted to higher angles, suggesting the partial substitution of large Pd atoms by smaller Cu atoms.[16] The composition of the 3D branched PdCu nanostructures prepared in standard conditions was confirmed by ICP-AES, from which the Cu content in the sample was measured to be 14 wt%. The electronic structure was analyzed by X-ray photoelectron spectroscopy (XPS). **Fig. S2a** shows the XPS spectra centered on the Pd 3*d* region. The two peaks located at 335.3 and 340.6 eV can be assigned to the metallic Pd $3d_{5/2}$ and Pd $3d_{3/2}$, whereas the peaks at 931.7 and 951.6 eV can be ascribed to the metallic Cu $2p_{3/2}$ and Cu $2p_{1/2}$ (**Fig. S2b**). The slight shifts in the binding energies of the 3D PdCu alloy compared to pure Pd (Pd $3d_{5/2}$: 335.0 eV) and Cu (Cu $2p_{3/2}$: 932.6 eV) suggest the presence of electronic interactions between Pd and Cu.[17]

In order to investigate the formation mechanism of the 3D branched PdCu nanostructures, various control experiments were set in order to assess the role of the reagents during the synthesis. As shown in **Fig. S3a**, in the case where no KBr was used (in the presence of HCl, 0.6 mmol), irregular PdCu nanoparticles were produced. By increasing the amount of KBr up to 10 mg, branched PdCu nanostructures start to appear (**Fig. S3b**). The desired 3D branched PdCu nanostructures could only be obtained after using more than 80 mg KBr (**Fig. S3c**). An excess amount of KBr (150 mg) caused the branched structure to overgrow, leading to the formation of PdCu nanostructures with much longer branches (**Fig. S3d**). The results suggest that the Br^- ions have a significant influence on the PdCu nanoarchitecture. It is well established that the Br^- ions preferentially adsorb on the (100) facets of *fcc* metals (e.g., palladium and copper alloy), which prevents growth along the <100> direction and is responsible for directing the formation of the nanowire construction.[18] In addition, when KBr is replaced by KCl or KI (in an equivalent molar ratio), irregular PdCu aggregates are obtained (**Fig. S4**). Consequently, only the use of Br^- ions as structure-directing agent can lead to the formation of branched PdCu nanostructures. The possible reason is that the binding strengths of halide ions to the Pd surface increase in the order of Cl^-<Br^-<I^-. As a result, weak chemisorption (Cl^-) or strong chemisorption (I^-) on the Pd surface are not favorable to the formation of branched structure.[18c,19]

The effect of HCl on the morphology of the PdCu nanostructures was also investigated. When the reaction was carried out in the absence of HCl, but in presence of 80 mg KBr, only irregular PdCu nanoparticles were obtained, owing to the fast reduction kinetics (**Fig. S5a**). When 0.3 or 0.6 mmol HCl is added to the reaction system, the precursor is reduced at a much lower reduction rate, as HCl tends to decrease the reduction capacity of ascorbic acid. In such case, the branched PdCu nanostructures can be obtained (**Fig. S5b,c**). Further increasing the amount of HCl (up to 1.2 mmol) yielded sea-urchin PdCu nanostructures with increased branch length (**Fig. S5d**). The increased branch length can be attributed to the decrease the number of seeds in the solution due to the slow reduction rate at initial stage. In addition, when HCl was replaced by equal amount of other strong acids (*e.g.*, HNO_3 or H_2SO_4), the 3D branched nanostructure could be well retained, indicating that the slow reduction kinetics induced by the presence of H^+, instead of the anions (*e.g.*, Cl^-, NO_3^-, SO_4^{2-}), takes the central role in the formation of 3D branched nanostructures (**Fig. S6a,b**).

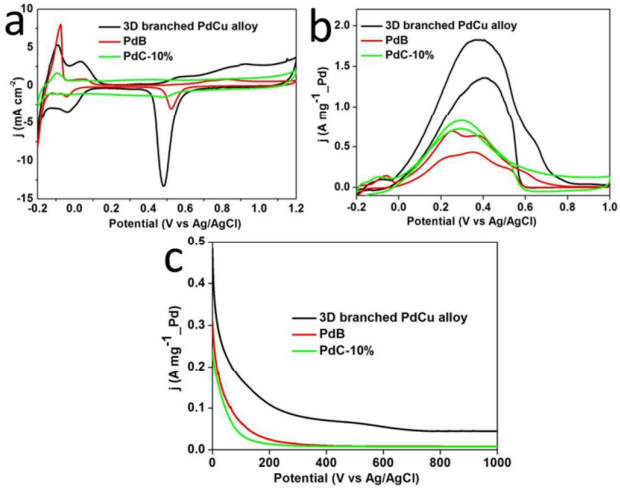

Fig. 3 Cyclic voltammograms of the 3D branched PdCu nanostructures, commercial PdB and PdC-10% samples in a) a 0.5 M $HClO_4$ solution and b) a mixture of 0.5 M $HClO_4$ and 0.5 M HCOOH at a scanning rate of 50 mV s^{-1}. c) Chronoamperometric curves for formic acid oxidation. The currents in panel a) are normalized by the electrode geometric surface area.

While Pd-based nanostructures are known to be efficient electrocatalysts for oxidizing organic fuel molecules, alloying them with 3d transition metals can greatly enhance their catalytic activity and stability. Herein, we selected the electrocatalytic oxidation of formic acid as a probe reaction to characterize the activity of the 3D branched PdCu nanostructures in acidic media. For comparison, commercial PdB and PdC-10% were selected as references under the same conditions. For comparison, commercial PdB and PdC-10% were selected as references under the same conditions. The cyclic voltammograms were recorded in the 0.5 M $HClO_4$ aqueous solution at a scanning rate of 50 mV s^{-1} (**Fig.3a**). The clear features of hydrogen desorption/adsorption (from 0.1 to -0.2 V) is an indication of the cleanliness of the catalytic surface. It is well known that the hydrogen atoms are essentially absorbed in the bulk Pd lattice by "dissolution adsorption mechanism".[20] The sharp peaks below 0 V is related to this dissolution adsorption process. The electrochemically active surface area (ECSA) of the Pd-based electrocatalysts cannot be precisely calculated by measuring the total charge passed in the "hydrogen region". Thus, we calculated the ECSA of the samples by integrating the charges associated with the PdO peak. The ECSA of the 3D branched PdCu nanostructures, commercial PdB and PdC-10% are 76.9 m^2 g^{-1}, 15.7 m^2 g^{-1}, and 37.3 m^2 g^{-1}, respectively. The results suggest that the 3D branched PdCu nanostructures provide a

much larger surface area and more catalytic active sites than others, as shown in **Table S1**. **Fig. 3b** shows the catalytic activity of the 3D branched PdCu nanostructures, commercial PdB and PdC-10% catalyst toward FAO in 0.5 M $HClO_4$ aqueous solution containing 0.5 M HCOOH. The current density was normalized by the Pd mass activities. The measured current density on the 3D branched PdCu nanostructure (1.84 A mg^{-1}_Pd) is about 2.7 and 2.2 times more than that of commercial PdB (0.69 A mg^{-1}_Pd) and PdC-10% catalyst (0.84 A mg^{-1}_Pd), respectively. The enhanced catalytic activity of the branched PdCu nanostructures is attributed to the large surface area which are provided by the assembly of 3D constructions and the synergistically enhanced electronic properties resulting from the alloy.[21] Compared to previously reported Pd-based catalysts (**Table S1**), our prepared 3D branched PdCu nanostructures also exhibit a higher current densities, showing the potential of this material for practical electrocatalytic applications such as formic acid oxidation. As an effective catalyst, the stability is a very important factor for fuel cells. Thus, the stability of catalysts was also investigated by chronoamperometric measurement for 1000 s in 0.5 M $HClO_4$ containing 0.5 M HCOOH. **Fig. 3c** clearly reveals that the branched PdCu nanostructures exhibited a slower current decay and a higher catalytic current intensity compared to the commercially available electrocatalysts. The high stability of the as-prepared 3D branched PdCu catalyst mainly originates from the one-dimensional structures, which suffers less from dissolution and aggregation (**Fig. S7**).

In summary, we successfully synthesized 3D branched PdCu nanostructures by a facile one-pot method. The simultaneous presence of HCl and KBr reagents is essential for the formation of 3D PdCu nanostructure. The as-prepared 3D branched PdCu nanostructures display an enhanced electrocatalytic activity and long-term stability toward the FAO compared to PdB or PdC-10%, which is mainly attributed to the unique structural features and the synergistic benefit from alloying Pd with Cu.

References

1 a) Q. Gao, Y. M. Ju, D. An, M. R. Gao, C. H. Cui, J. W. Liu, H. P. Cong, S. H. Yu, *ChemSusChem*, 2013, **6**, 1878; b) K. Qi, Q. Wang, W. Zheng, W. Zhang, X. Cui, *Nanoscale*, 2014, **6**, 15090.

2 a) H. Wang, S. Ishihara, K. Ariga, Y. Yamauchi, *J. Am. Chem. Soc.,* 2012, **134**, 10819; b) T. Yu, D. Y. Kim, H. Zhang, Y. Xia, *Angew. Chem. Int. Ed.*, 2011, **50**, 2773; c) X. Huang, Z. Zhao, J. Fan, Y. Tan, N. Zheng, *J. Am. Chem. Soc.,* 2011, **133**, 4718.

3 K. Sasaki, H. Naohara, Y. M. Choi, Y. Cai, W. F. Chen, P. Liu, R. R. Adzic, *Nat. Commun.*, 2012, **3**, 1115.

4 a) Y. Jia, Y. Jiang, J. Zhang, L. Zhang, Q. Chen, Z. Xie, L. Zheng, *J. Am. Chem. Soc.,* 2014, **136**, 3748; b) S. Chen, H. Su, Y. Wang, W. Wu, J. Zeng, *Angew. Chem. Int. Ed.,* 2015, **54,** 108; c) Z, Zhang, Y. Yang, F. Nosheen, P. Wang, J. Zhang, J. Zhuang, X. Wang, *Small,* 2013, **9**, 3063; d) Y. Wu, D. Wang, G. Zhou, R. Yu, C. Chen, Y. Li, *J. Am. Chem. Soc.,* 2014, **136**, 11594.

5 a) K. A. Kuttiyiel, K. Sasaki, D. Su, L. Wu, Y. Zhu, R. R. Adzic, *Nat. Commun.,* 2013, **52,** 5185; b) S. Liu, Q. Zhang, Y. Li, M. Han, L. Gu, C. Nan, J. Bao, Z. Dai, J. *Am. Chem. Soc.*, 2015, **137**, 2820.

6 a) V. Mazumder, M. Chi, M. N. Mankin, Y. Liu, Ö. Metin, D. Sun, K. L. More, S. Sun, *Nano Lett.*, 2012, **12**, 1102; b) S. Ha, R. Larsen, R. I. Masel, *J. Power Sources,* 2005, **144**, 28.

7 C. Hu, X. Zhai, Y. Zhao, K. Bian, J. Zhang, L. Qu, H. Zhang, H. Luo, *Nanoscale*, 2014, **6**, 2768.

8 a) S. Guo, S. Dong, E. Wang, *ACS Nano*, 2010, **4**, 547; b) J. Xie, Q. Zhang, W. Zhou, J. Y. Lee, D. I. C. Wang, *Langmuir*, 2009, **25**, 6454; c) Y. B. He, G. R. Li, Z. L. Wang, Y. N. Ou, Y. X. Tong, *J. Phys. Chem. C*, 2010, **114**, 19175.

9 a) B. Y. Xia, H. B. Wu, N. Li, Y. Yan, X. W. Lou, X. Wang, *Angew. Chem. Int. Ed*., 2015, **54**, 3797; b) B. Lim, Y. Xia, *Angew. Chem. Int. Ed.*, 2011, **50**, 76; c) X. Yu, D. Wang, Q. Peng, Y. Li, *Chem. Eur. J.,* 2013, **19**, 233; d) H. S. Chen, Y. T. Liang, T. Y. Chen, Y. C. Tseng, C. W. Liu, S. R. Chung, C. T. Hsieh, C. E. Lee, K. W. Wang, *Chem. Commun.*, 2014, **50**, 11165.

10 a) M. Rauber, I. Alber, S. Müller, R. Neumann, O. Picht, C. Roth, A. Schökel, M. E. Toimil-Molares, W. Ensinger, *Nano Lett.,* 2011, **11**, 2304; b) N. C. Bigall, A. K. Herrmann, M. Vogel, M. Rose, P. Simon, W. Carrillo-Cabrera, D. Dorfs, S. Kaskel, N. Gaponik, A. Eychmüller, *Angew. Chem. Int. Ed.,* 2009, **48**, 9731; c) F. Yu, W. Zhou, R. M. Bellabarba, R. P. Tooze, *Nanoscale,* 2014, **6**, 1093.

11 B. Y. Xia, W. T. Ng, H. B. Wu, X. Wang, X. W. Lou, *Angew. Chem. Int. Ed.*, 2012, **51**, 7213.

12 a) M. Bersani, L. Conte, A. Martucci, M. Guglielmi, G. Mattei, V. Bello, R. Rosei, M. Centazzo, *Nanoscale*, 2014, **6**,1560; b) C. Xu, Q. Hao, H. Duan, *J. Mater. Chem. A,* 2014, **2**, 8875; c) J. J. Lv, L. P. Mei, X. Weng, A. J. Wang, L. L. Chen, X. F. Liu, J. J. Feng, *Nanoscale*, 2015, **7**, 5699; d) Y. W. Lee, M. Kim, S. W. Kang, S. W. Han, *Angew. Chem. Int. Ed.,* 2011, **50**, 3466.

13 S. F. Ho, A. Mendoza-Garcia, S. Guo, K. He, D. Su, S. Liu, Ö. Metin, S. Sun, *Nanoscale*, 2014, **6**, 6970.

14 a) L. Ma, C. Wang, M. Gong, L. Liao, R. Long, J. Wang, D. Wu, W. Zhong., M. J. Kim, Y. Chen, Y. Xie, Y. Xiong, ACS Nano, 2012, **6**, 9797; b) S. Maksimuk, X. Teng, H. Yang, *J. Phys. Chem. C*, 2007, **111**, 14312.

15 a) Y. H. Chen, H. H. Hung, M. H. Huang, *J. Am. Chem. Soc.,* 2009, **131**, 9114; b) B. Jiang, C. Li, M. Imura, J. Tang, Y. Yamauchi, *Adv. Sci.*, 2015, **2**, 201500112.

16 a) Y. Zheng, S. Zhao, S. Liu, H. Yin, Y. Y. Chen, J. Bao, M. Han, Z. Dai, *ACS Appl. Mater. Interfaces*, 2015, **7**, 5347; b) H. H. Li, C. H. Cui, S. Zhao, H. B. Yao, M. R. Gao, F. J. Fan, S. H. Yu, *Adv. Energy Mater*. 2012, **2**, 1182; c) B. Jiang, C. Li, V. Malgras, Y. Yamauchi, *J. Mater. Chem. A,* 2015, **3**, 18053.

17 a) Z. Y. Shih, C. W. Wang, G. Xu, H. T. Chang, *J. Mater. Chem. A*, 2013, **1**, 4773; b) C. Xu, Y. Liu, J. Wang, H. Geng, H. Qiu, *J. Power Sources*, 2012, **199**, 124.

18 a) K. Zhang, D. Bin, B. Yang, C. Wang, F. Ren, Y. Du, *Nanoscale*, 2015, **7**, 12445; b) L. Zhang, S. I. Choi, J. Tao, H. C. Peng, S. Xie, Y. Zhu, Z. Xie, Y. Xia, *Adv. Funct. Mater*., 2014, **24**, 7520; c) M. Chen, B. Wu, J. Yang, N. Zheng, *Adv. Mater*. 2012, **24**, 862.

19 F. Wang. C. Li, L. D. Sun, C. H. Xu, J. Wang, J. C. Yu, C. H. Yan, *Angew. Chem. Int. Ed.,* 2012, **51**, 4872.

20 a) J. Y. Wang, Y. Y. Kang, H. Yang, W. B. Cai, *J. Phys. Chem. C,* 2009, **113**, 8366; b) D. Sun, L. Si, G. Fu, C. Liu, D. Sun, Y. Chen, Y. Tang, T. Lu, *J. Power Sources*, 2015, **280**, 141; c) M. Breiter, *J. Electroanal. Chem. Interfacial Electrochem*., 1977, **81**, 275.

21 a) Q. S. Chen, Z. N. Xu, S. Y. Peng, Y. M. Chen. D. W. Lv, Z. Q. Wang, J. Sun, G. C. Guo, *J. Power Sources,* 2015, **282**, 471; b) H. Wu, H. Li, Y. Zhai, X. Xu, Y. Jin, *Adv. Mater*. 2012, **24**, 1594.